A hybrid subnano cluster electrocatalysis process for recalcitrant wastewater treatment

Li, Biao; Zou, Rusen; Su, Yanyan; Zhang, Yifeng

Published in:
Separation and Purification Technology

Link to article, DOI:
10.1016/j.seppur.2022.122372

Publication date:
2023

Document Version
Publisher's PDF, also known as Version of record

Separation and Purification Technology 304 (2023) 122372

Contents lists available at ScienceDirect

Separation and Purification Technology

journal homepage: www.elsevier.com/locate/seppur

A hybrid subnano cluster electrocatalysis process for recalcitrant wastewater treatment

Biao Li [a], Rusen Zou [a], Yanyan Su [b,*], Yifeng Zhang [a,*]

[a] Department of Environmental and Resource Engineering, Technical University of Denmark, DK-2800 Lyngby, Denmark
[b] Carlsberg Research Laboratory, Bjerregaardsvej 5, Valby 2500, Denmark

ARTICLE INFO

Keywords:
Subnano clusters
Advanced oxidation processes
Wastewater treatment
Filter
Electrochemical system

ABSTRACT

Metal clusters are emerging as efficient H_2O_2 activators to remove organic pollutants in advanced oxidation processes. However, these processes are still dependent on particle size and large doses of H_2O_2. To solve these issues, more uniform small-size catalysts that require less H_2O_2 and in-situ H_2O_2 synthesis should be pursued. Here we employed a simple way to synthesize subnano FeN_x clusters and demonstrated its high activity for multiple pollutant removal even at low H_2O_2 concentrations and a wide pH range. These excellent properties motivated us to further immobilize it in a filter, achieving nearly 100% pollutant degradation and H_2O_2 utilization. Moreover, a full-body hydrophobic engineered cathode was developed for stable in-situ H_2O_2 electrosynthesis over 320 h. The H_2O_2 generation cell can be integrated with the Fenton filter to realize comprehensive improvements in efficacy, sustainability, application potential, and reduction of operating costs. This study offers insight into integrating metal clusters with electrochemical systems for high efficiency and low-cost treatment of recalcitrant wastewater.

1. Introduction

Advanced oxidation processes (AOPs), which generate reactive radicals (e.g., $^{\bullet}OH$, $SO_4^{\bullet-}$, $Cl^{\bullet}$, and $^1O_2$) via activating various oxidants, have been considered efficient and eco-friendly technologies for wastewater treatment and subsurface contamination remediation [1–3]. For example, due to the high activity and non-selectivity of $^{\bullet}OH$ ($k = 10^9$ M^{-1} s^{-1}), Fenton or Fenton-like reactions can oxidize numerous toxic and stubborn contaminants and finally mineralize them into harmless molecules (CO_2 and H_2O) [4,5]. Although the H_2O_2-based AOPs processes have been defined for over 30 years, key limitations still exist.

The first limitation is the low catalytic efficiency of catalysts. Classical homogeneous catalysts (HMCs) can activate H_2O_2 via Fe^{2+}/Fe^{3+} redox cycle (40–80 M^{-1} s^{-1}), yet face problems of narrow pH range, metal-rich sludge production, and poor reusability [6,7]. As competitive alternatives, metal-based heterogeneous catalysts (HTCs) exhibit relatively tepid reaction kinetics (typically 0.01–0.2 min^{-1}) and moderate pH adaptability (typically 3–9) [8–10]. Unfortunately, they do not truly break through the pH and real-world limitations, significantly hindering their large-scale applications [11,12]. On the one hand, the adopted acidic conditions can cause fast leaching of metal ions, while the formation of sludge and the deactivation of $^{\bullet}OH$ may occur at high pH [3,13]. On the other hand, various types of components in actual wastewater can slow down the Fenton reaction by covering the active sites, competing for H_2O_2 utilization, and quenching $^{\bullet}OH$ [14,15].

The second limitation is the in-situ generation of H_2O_2 according to the needs. The current anthraquinone technology for H_2O_2 production follows a complex procedure that requires a vast energy supply, and thus, is not suitable for large-scale implementation [4,16]. Moreover, the transportation and storage of concentrated H_2O_2 is a hazardous process that further impedes its applications in remote communities [16]. Recently, the in-situ electrochemical synthesis of H_2O_2 from $2e^-$ oxygen reduction reaction (ORR) has attracted intensive attention in labs and industries [17]. Although substantial efforts have been invested in catalyst preparation and cathode fabrication [18–20], few studies have shown the practical utility of H_2O_2-AOPs at device levels. Low H_2O_2 dosage cannot meet the treatment requirements of high COD wastewater, while excessive H_2O_2 introduction needs post-treatment of the effluent [4]. Thus, long-term synthesis of H_2O_2 in the target range could be the best option for AOPs applications.

Metal clusters are emerging as research frontiers owing to stable metal-support interactions, high active site exposure, and excellent

* Corresponding authors at: FMC Agricultural Solutions Danmark, Genvej 2, 2970 Hørsholm, Denmark (Y. Su).
E-mail addresses: yanyansu@daad-alumni.de (Y. Su), yifz@dtu.dk (Y. Zhang).

https://doi.org/10.1016/j.seppur.2022.122372
Received 22 August 2022; Received in revised form 3 October 2022; Accepted 9 October 2022
Available online 17 October 2022

activity [21,22]. Given these, they have proven to be a better solution than classical HMCs and HTCs to overcome the first challenge [9,23]. However, these processes are catalyst size-dependent and initially require high concentrations of H_2O_2 (usually > 10 mM), leading not only to unclear interactions between clusters and H_2O_2, but also to low utilization, high cost, and complex operations. Moreover, few studies have focused on the application of metal clusters in practical wastewater treatment, not to mention long-term testing in continuous models. Therefore, there is an urgent need to synthesize metal clustes at the same scale, and develop a metal cluster-combined system with controllable H_2O_2 synthesis, efficient H_2O_2 activation, and long-time stability.

In this study, we integrated and evaluated uniform subnano FeN_x clusters with an electrochemical system to realize sustainable generation and simultaneous activation of H_2O_2 for water treatment. Firstly, we simply prepared FeN_x clusters at the same sub-nanoscale, enabling efficient cluster-H_2O_2 interactions and high multi-organic oxidation kinetics even at a low H_2O_2 dosage (0.875 mM) and high initial pH (9). The device-level application potential of the clusters was tested by immobilizing the clusters in a simple Fenton filter and continuously flowing actual wastewater through it. Furthermore, we integrated the FeN_x cluster filter with an in-situ electrosynthesis H_2O_2 system for efficient, long-term stable, and low-cost water treatment. Our work provides profound insights into subnano cluster design and efficacy improvement and its practical application in electrochemical AOPs.

2. Materials and methods

2.1. Chemicals

$FeCl_3{\cdot}6H_2O$ and dicyandiamide were used as precursors for catalyst synthesis. Multiple organic chemicals including methylene blue (MB), meldola's blue (MeB), toluidine blue (TB), metyl orange (MO), orange G (OG), p-hydroxybenzoic acid (HBA), pyrocatechol (PRC), and ibuprofen (BF) were chosen as representative pollutants·H_2O_2, NaCl, $NaHCO_3$, K_3PO_4, and coumarin were used in the batch experiments. In addition, carbon black (CB) and poly-tetra-fluoroethylene (PTFE) were used for electrode preparation in electrochemical systems. Chemicals were purchased from Sigma-Aldrich if not otherwise specialized.

2.2. Development of three systems

2.2.1. Batch system

The FeN_x cluster was synthesized by a co-pyrolysis method. In detail, different masses of dicyandiamide (0.5, 1.0, 1.5, and 2.0 g) were mixed with a fixed amount of $FeCl_3{\cdot}6H_2O$ (0.35 g) in the mortar, respectively. Next, 1 mL H_2O was dropped into the mortar and then ground to a mushy mixture. The mixture was transferred into a small-mouth glass vial and covered with aluminum foil. Subsequently, the vials were placed into a muffle furnace heated to 550 °C at 10 °C/min and maintained at the highest temperature for 2 h. Different colours of solid catalysts (named $FeN_{0.5}$, $FeN_{1.0}$, $FeN_{1.5}$, and $FeN_{2.0}$) were finally obtained and ground for later use.

In a typical batch system, 5.0 mg of catalyst was added into a glass beaker (50 mL) along with synthetic MB wastewater (10 mL, 20 mg/L, pH 7). Then 2.625 mM H_2O_2 was introduced to start the Fenton-like reaction at a rotation speed of 200 rpm. The effects of different catalysts (FeN_x, x = 0.5–2.0), H_2O_2 concentrations (0.875–3.5 mM), pH (3–11), and catalyst contents (1.0–5.0 mg) on system performance were also studied. For the degradation of synthetic dye wastewater, 200 μL solution was withdrawn at fixed time intervals and mixed with 100 μL methanol and then immediately measured on a microplate reader (Synergy™ HTX) at different wavelengths (MB, 665 nm; MeB, 570 nm; TB, 635 nm; MO, 465 nm; OG, 475 nm). The degradation procedure of phenolic compounds and drugs was the same as the dyes, except that 1 mL samples were withdrawn and analyzed (see detail in Table S1). The influences of anions and water sources on the catalyst activity were performed by adding Cl^-, HCO_3^-, and PO_4^{3-} (0.1 M, 100 μL each) and using deionised water (DI water), tap water, and real wastewater (Lyngby wastewater treatment plant, Denmark, Table S2).

2.2.2. Flow-through system

The flow-through system consists of a Fenton filter and a wastewater tank connected by a pump. The filter was developed by assembling eight pieces of catalyst-modified carbon felts (CF) into a plastic column (15 × 3.5 cm). Firstly, CF was cut into pancakes (4 × 0.5 cm) and pre-treated with H_2SO_4 solution (1 M) overnight to remove impurities on the CF surface. After washing several times with DI water, the CF was dried and immersed in the mixed precursor solution (0.35 g $FeCl_3{\cdot}6H_2O$, 1.0 g dicyandiamide, and 10 mL H_2O) until the CF fully adsorbed the mixed solution. Then the wet CF was moved into a muffle furnace and underwent the same procedure as in Section 2.2.1.

The synthetic MB wastewater (5–10 mg/L, pH 7, 5 L) was dosed with H_2O_2 (1.75–2.625 mM) and then flowed through the Fenton filter at different speeds (0.05–0.1 L/h). To test the application potential of the filter, H_2O_2 (2.625 mM) was added into MB solution (10 mg/L, pH 7, 5 L) and then mixed with the abovementioned wastewater without pH adjustment and then filtrated at a speed of 0.05 L/h. The concentrations of H_2O_2 and MB were analyzed after the filtration.

2.2.3. Electrochemical integration system

The integrated electrochemical system comprises three parts: wastewater tank, H_2O_2 generation cell, and Fenton filter. The first and last parts are the same as in section 2.2.2. The second part is a dual-chamber electrochemical system. A commercial anode (IrO_2/Ti, 4 × 4 cm) and a facile cathode (full-body functionalized CF, 4 × 4 cm) were prepared and separated by a cation exchange membrane (CEM). The cathode was developed by immersing the pre-treated CF in a mixture solution of carbon black (100 mg) and PTFE (5%, 12 mL). Then the fully absorbed CF was heated in a muffle furnace at 360 °C for 30 min. As a comparison, different concentrations of PTFE (0–8%) were also used for CF functionalization.

The controllable in-situ generation of H_2O_2 was investigated by changing the external voltage (1.5–2.4 V), the concentration and pH of the catholyte (Na_2SO_4, 0.05–0.1 M, pH 3–9), and the flow rate (0.05–0.1 L/h). The stability of the system was tested for over 320 h at the optimal condition (0.05 M Na_2SO_4, pH 7, 1.6 V, 0.05 L/h).

The performance of the integration system was further evaluated under different concentrations of Na_2SO_4 (0.05–0.1 M) and MB (5–10 mg/L), different flow rates (0.05–0.1 L/h), and different external voltage (1.6–2.0 V). During these processes, the concentrations of MB and H_2O_2 before and after filtration were measured. In addition, the actual wastewater after secondary treatment was mixed with MB solution and pumped through the filter to test the application potential of the integrated system.

2.3. Characterization and chemical analysis

The morphology, composition and structure of FeN_x catalysts were characterized by transmission electron microscopy (TEM, Tecnai T20 G2) with energy-dispersive X-ray spectroscopy (EDS), High-angle annular dark-field scanning transmission electron microscopy (HAADF-STEM), and X-ray diffraction (XRD, PANalytical) with Cu Kα X-ray source. In addition, the surface chemical states of the catalysts were determined by X-ray photoelectron spectroscopy (XPS, K-Alpha, ThermoFisher) and Fourier transform infrared spectroscopy (FTIR, NicoletiS50, ThermoFisher).

Electrochemical characterization of the anode (via cyclic voltammetry, CV) and cathode (via linear sweep voltammetry, LSV) were performed by an electrochemical workstation (IVIUMnSTAT) (see detail in Text S1). The organic concentration was tested by HPLC (Agilent, USA) and TOC (Shimadzu, Japan). H_2O_2 concentration was detected as previously reported [20]. The concentration of Fe leaching was

measured by an inductively coupled plasma optical emission spectrometer (ICP-OES, Agilent). Coumarin was selected as a fluorescent probe to detect the generation of ·OH [24].

3. Results and discussion

3.1. Performance of the batch system

3.1.1. Characterization of FeN_x clusters

FeN_x (x = 0.5–2.0) was synthesized via co-pyrolysis of the grinding mixture precursors containing fixed $FeCl_3$ and different amounts of dicyandiamide (Fig. S1). This two-step strategy is beneficial for the complete interaction of precursors and the uniform accommodating of Fe clusters by nitrogen anchors. TEM image shows no prominent spot distribution on $FeN_{1.0}$ with a smooth body and rough edge (Fig. 1a), indicating that the Fe sites were well dispersed and no nanoparticles formed. We also did not observe nano-sized catalysts with different dicyandiamide dosages (0.5–2.0 g), implying the general synthesis of FeN_x at the same subnano scale (Fig. S2a–c). HAADF-STEM image further confirmed the even distribution of Fe clusters on $FeN_{1.0}$. As shown in Fig. 1b, many light spots are star-like embellished on the support without aggregation. To discern the spatial distribution of Fe clusters on the nitrogen support, we converted a HAADF-STEM image into a 3D pseudo-colour surface map. Fig. 1c exhibits that subnano Fe particles are printed as isolated yellow spikes and dispersedly anchored on the entire support (green layer). Moreover, elemental mapping manifested similar steady tendency signals for the three main elements (Fig. 1d and S2d–e), indicating non-selective isolation of subnano Fe particles by sufficient nitrogen sites.

The XRD spectrum of FeN_x (x = 1.0–2.0) did not display obvious Fe species peaks, while negligible Fe_2O_3 peaks could be found on $FeN_{0.5}$ (Fig. 1e) [25]. It agreed well with previous studies and suggested the importance of accurately controlling the ratio of precursors for subnano cluster synthesis [26]. More importantly, we observed that the identified peak of the support gradually declined and left-shifted with the decrease of nitrogen precursor usage, indicating efficient Fe cluster-support interactions [27]. A similar result was also found in FT-IR spectroscopy analysis. The characteristic peaks of the support at the yellow regions (particularly at 810 and 1314 cm^{-1}) all declined progressively, implying the *N*-coordination of Fe clusters on the support (Fig. 1f) [28,29]. XPS was further used to study the surface electronic properties of these catalysts. The peak intensities of Fe $2p_{1/2}$ and Fe $2p_{3/2}$ significantly declined and the peak positions shifted left to higher binding energies at higher nitrogen content (Fig. 1g), which agreed well with the XRD results and confirmed the dispersion of Fe sites and the change of Fe valence [29]. Even though the content of Fe and O decreased, N content increased (Fig. 1h). The high resolution of N1s spectra was further deconvoluted into three peaks: pyridinic N (398.2 eV), pyrrolic N (399.9 eV), and graphitic N (401.1 eV) (Fig. S1f) [30]. Pyridinic N has been widely reported as the main anchor to bind Fe sites [27,31]. We found that its percentage decreased with increasing nitrogen content (Fig. S2f), suggesting that more bonded Fe sites were formed on $FeN_{0.5}$. Thus, precisely controlling the ratio of N and Fe precursors within a specific range could be a facile and effective strategy to disperse Fe sites to subnano scales via active nitrogen anchors.

3.1.2. Degradation of multiple pollutants

To evaluate the catalytic activity of subnano FeN_x cluster, we first selected the oxidation of MB as a model Fenton-like reaction. As depicted in Fig. 2a, the catalyst efficacy decayed with increasing support content. Especially, $FeN_{0.5}$ reached almost 100% MB removal efficiency within 10 min, while only 38.41% of MB was removed in the $FeN_{2.0}$/H_2O_2 system, indicating the promotion role of more Fe active sites at the same scale. We also found that all catalysts exhibited a two-stage catalytic process. The efficiencies in the first stage (accounting for 38.35–94.40% within 2 min) were significantly higher than that of the second stage (2–20 min). It could be attributed to the high concentration of H_2O_2 and a large number of active sites in the first stage, which were consumed in the following process. The degradation efficiencies and rates achieved by $FeN_{0.5\text{-}1}$ were also among the best in published works (Table S3). To further compare their activities, the modified concepts of active sites (AS), turnover number (TN), and turnover frequency (TF) were introduced (detailed in Text S1). Fig. 2b shows a similar decrease trend in AS. In contrast, the TN and TF of these catalysts increased at $FeN_{0.5\text{-}1.5}$ but decreased at $FeN_{2.0}$ (Table S4), suggesting that there was a balanced number in N_x ($1.0 \leq X \leq 2.0$) to achieve the highest efficacy of each site. Additionally, the reduced H_2O_2 utilization efficiency (from 96.87% to 38.66%, Fig. 2c) in different catalyst/H_2O_2 systems linearly matched the above catalytic activities (Fig. S3a), implying that rapid MB removal benefited from efficient H_2O_2 utilization. We have previously

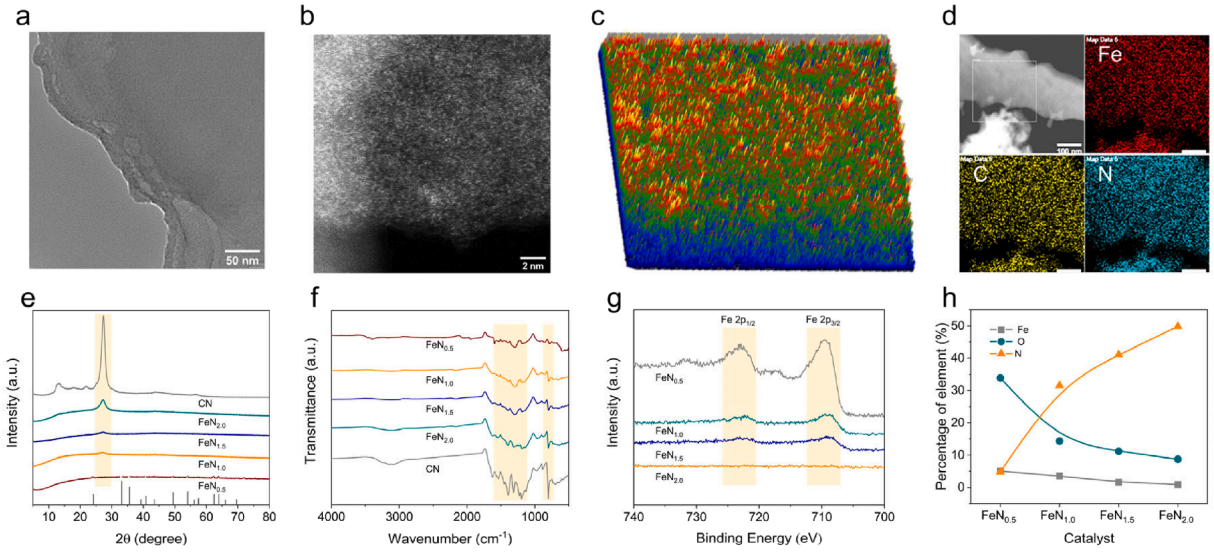

Fig. 1. (a) TEM image of $FeN_{1.0}$ without the existence of obvious nanoparticles. (b) HAADF-STEM of $FeN_{1.0}$ with light clusters. (c) 3D pseudo-color surface map of $FeN_{1.0}$ with subnano Fe clusters printed as yellow spikes. (d) EDS mapping images of $FeN_{1.0}$ with uniform distribution of Fe, C, and N. (e) Wide-angle XRD patterns (inset of standard peaks of Fe_2O_3), (f) FTIR spectra, (g) Fe 2p XPS spectra, and (h) different element contents of the obtained catalysts. (For interpretation of the references to color in this figure legend, the reader is referred to the web version of this article.)

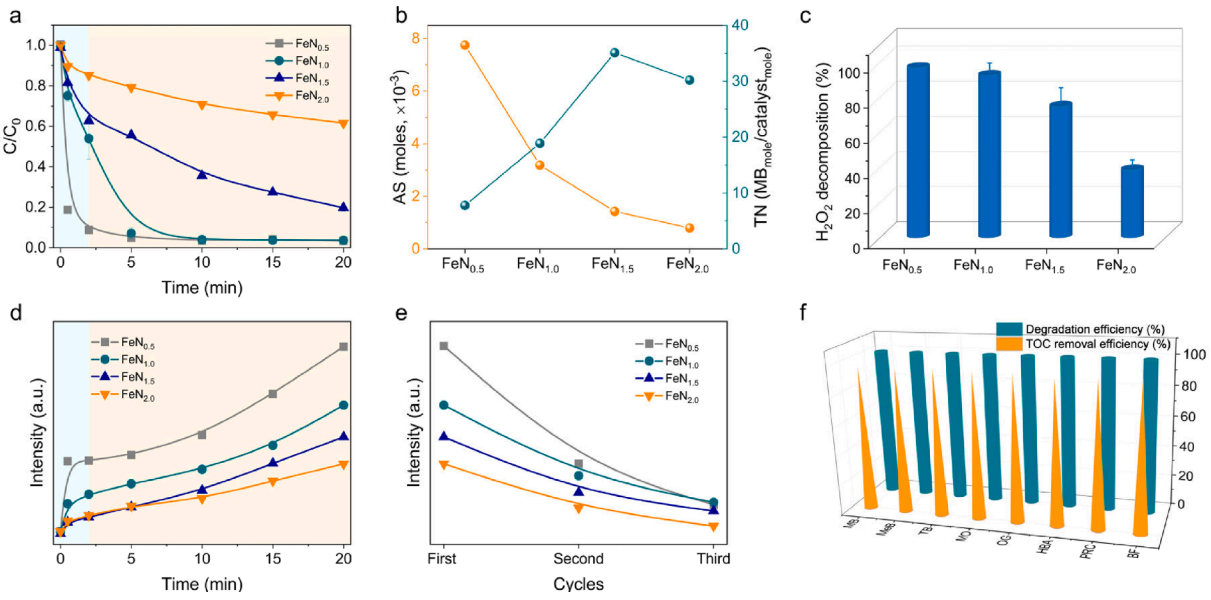

Fig. 2. (a) Two-stage degradation of MB, (b) the number of active sites and turnover, (c) H_2O_2 utilization efficiency, (d) ˙OH accumulation, and (e) ˙OH decline in three cycles in the batch system with different catalysts. (f) Degradation and TOC removal efficiencies of 20 mg/L dyes (MB, MeB, TB, MO, and OG), phenolic compounds (HBA and PRC), and drug (BF) achieved by the $FeN_{1.0}$-H_2O_2 catalytic system. Reaction conditions: catalyst (0.5 g/L), MB (20 mg/L), H_2O_2 (2.265 mM) and initial pH (7), if not otherwise specialized.

demonstrated that dissolved Fe and conventional nano-catalysts show relatively low catalytic capability even at high concentrations [26]. These results supported that subnano clusters are suitable catalysts to reveal the relationship between H_2O_2 utilization and pollutant oxidation.

The generation of ˙OH was detected to affirm the above linear relationship as solid evidence. Fig. 2d and S3b show that the fluorescence intensity of 7-hydroxycoumarin (the product of ˙OH and coumarin) increased in all systems and achieved the highest value by $FeN_{0.5}$. Interestingly, the change of ˙OH intensity also followed a two-stage process. The exponential rises in the first stage and the linear rises in the second stage were consistent with catalyst efficiency trends (Fig. 2a). Furthermore, the highest intensity at 20 min also linearly dropped with increasing nitrogen content, demonstrating the great contribution of ˙OH during the FeN_x/H_2O_2 Fenton-like process. However, we found a different downward trend in ˙OH intensity when using these catalysts. Although $FeN_{0.5}$ showed the best activity in the initial stage, its ˙OH accumulation extremely declined by 67.48% after three cycles (Fig. 2e). The intensities of $FeN_{1.0}$, $FeN_{1.5}$, and $FeN_{2.0}$ were reduced by 55.19%, 51.28%, and 52.90%, respectively. The sharp decline of $FeN_{0.5}$ stability could be due to the high Fe leaching in the first cycle. As presented in Fig. S4a, the Fe leaching in $FeN_{0.5\text{-}2.0}$ dropped from 156.1 to 19.5 μg/L, which was also linearly bonded with the decreasing content of Fe in different catalysts (5.02–0.89%, XPS results). According to our previous studies, high Fe leaching could improve Fenton efficiency via homogeneous reaction [26]. However, we discovered the disadvantage of high Fe leaching in repeated applications in this study. Note that the ˙OH intensity in the $FeN_{1.0}/H_2O_2$ system attained the highest peak. The total Fe leaching rate of $FeN_{1.0}$ was only 1.16% after three reaction cycles. Moreover, catalyst properties (e.g., catalyst morphology and distribution of the clusters) remained almost unchanged (data not shown). These further enlighten us to control the number of catalytic sites to achieve high efficiency and long-term stability in wastewater treatment. Thus, $FeN_{1.0}$ was determined to be a better catalyst and used in the following experiments.

The catalytic applicability of the $FeN_{1.0}/H_2O_2$ system was evaluated by using multiple environmental pollutants as targets, including industry dyes (MeB, TB, MO, and OG), phenolic compounds (HBA and PRC), and drug (BF). As expected, these organic pollutants were all efficiently degraded and eventually mineralized, as suggested by 100% degradation efficiencies and above 90% TOC removal efficiencies within 30 min (Fig. 2f). To verify the presence of Fe active sites and the dominant role of ˙OH, we introduced oxalate and TBA as the chelator of Fe and the chemical probe of ˙OH, respectively (Fig. S4c–d). With their concentrations increased, both chemicals inhibited the catalytic activity, revealing the involved catalytic mechanism with subnano Fe clusters as the activator for H_2O_2 activation and ˙OH as the free radical for pollutant oxidation. We also studied the role of other radicals in this catalytic system. While the addition of FFA resulted in the decrease of pollutant removal, the role of $^1O_2$ cannot be highlighted due to FFA can also react with ·OH (1.5×10^{10} M^{-1} s^{-1}), and we only measured a weak signal of the generated $^1O_2$ (Fig. S5). The role of other radicals (e.g., $O_2^{\cdot}$) was not significant since we observed negligible signals.

3.1.3. *Effects of operating parameters*

In the classical Fenton treatment system, H_2O_2 is typically added in high doses, which suffers from self-decomposition and low utilization [32]. An effective way to solve these issues is to reduce H_2O_2 concentration while ensuring that H_2O_2 is efficiently activated for ˙OH generation. In light of the high activity of FeN_x clusters, we fed low doses of H_2O_2 (significantly lower than more previous studies) and evaluated their impact on system performance. The results showed that MB was almost completely removed at all tested H_2O_2 concentrations. Specifically, MB degradation efficiency increased with H_2O_2 concentration (0.875–2.625 mM) and slightly reduced at 3.5 mM. (Fig. S6a). Additionally, the data were well fitted to positive lines by the pseudo-first-order model (PFO, $R^2 > 0.97$), and the corresponding apparent rate constants (0.011–0.063 min^{-1}) matched the degradation efficiencies (Fig. S6b). More importantly, the H_2O_2 utilization was over 90% in all systems (Fig. S6c), independent of pH conditions, as pH showed a similar tendency throughout the reaction (Fig. S6d). The highest value observed at 3.5 mM H_2O_2 could be attributed to the fact that excess H_2O_2 can react with ˙OH, thereby hindering the Fenton process [32].

The pH adaptability of Fenton catalysts is another essential factor [33,34]. As shown in Fig. S7a, MB was efficiently oxidized in the pH range of 3–7, and the efficiencies of 88.91% and 49.84% can still be obtained even in the range of 9–11, indicating the substantial pH adaptability of FeN_x over classical HMCs and HTCs [33,34]. The PFO

lines were also well fitted and consistent with the degradation efficiencies (Fig. S6a, inset). Similarly, the catalytic activity of the system was linearly bonded to H_2O_2 utilization (96.55–42.28%) at different pH (Fig. S7b), indicating the interconnected relationship between them. Note that we found a pH drop same as our previous work [31]. When $FeN_{1.0}$ was added to the system, the pH of the solution decreased (Fig. S7c), indicating that the catalyst had the ability to acidify the solution. Especially the pH was kept at the acidic region in the range of 3–9, providing a suitable environment for the Fenton reaction. However, the pH adjustment ability was inhibited at high pH values (9–11), resulting in decreased efficiencies. These results were further confirmed by the zeta potential of the catalyst in the solution with different pH conditions (Fig. S7d). With more active sites, high content of $FeN_{1.0}$ can activate H_2O_2 more efficiently, thus generating more $^{\bullet}OH$ for MB oxidation (Fig. S8a). It was further verified by the increased apparent rate constant (0.016–0.31 min^{-1}, Fig. S8b) and H_2O_2 utilization (41.20–92.53%, Fig. S8c) and the linear interrelationship between them. Meanwhile, high catalyst contents seem to help the pH reduction (Fig. S8d).

Furthermore, we studied the catalyst activity in the presence of common anions (Cl^-, HCO_3^-, and PO_4^{3-}) and different water sources. Similar to previous reports, the obtained FeN_x cluster in this study did not overcome the influence of the water matrix [15]. Consequently, MB degradation was significantly reduced to 79.37–28.99% by anions (Fig. S9a) and 49.37–25.53% by water sources (Fig. S9b). This could be due to organic compounds in this water may compete for H_2O_2 utilization while inorganic compounds could undesirably quench $^{\bullet}OH$ [15]. We also noticed that the introduction of anions or wastewater seriously impacted the pH change of the solution (Fig. S9c–d). We have demonstrated that higher alkalinity solutions were less prone to be acidified by the catalyst, thus damaging the acidic environment of the $FeN_{1.0}/H_2O_2$ system and reducing the Fenton efficiency [26].

3.2. Flow-through filter for wastewater treatment

Inspired by membrane-based filtration, we assembled a flow-through filter to improve the lifespan and stability of FeN_x clusters. The working principle of the filter is illustrated in Fig. 3a. Wastewater can flow through the micropores of the catalyst-modified CF without the help of gas pressure. After the Fenton-like reaction occurs across the CF, the organics in wastewater can be gradually oxidized layer by layer. SEM images exhibit that the catalyst grows irregularly on the surface of each piece of CF, integrating a cross-network for rapid H_2O_2 activation and pollutant degradation (Figs. 3b and S10). Driven by a pump, the synthetic MB wastewater (10 mg/L, 5 L, pH 7) was mixed with H_2O_2 (2.265 mM) and then filtrated through the filter at a flow rate of 0.1 L/h. The results showed that almost complete removal (>95%) was obtained by a single pass throughout the filtration process (Fig. 3d). Meanwhile, H_2O_2 was also consumed efficiently, achieving a win–win outcome. In contrast, the filter without catalyst modification had a negligible contribution to the pollutant degradation, suggesting the relatively low adsorption effect of CF and weak oxidation power of solely H_2O_2 (data not shown).

We also conducted experiments under different conditions to compare with the above batch system. Firstly, when the H_2O_2 concentration was increased to 3.5 mM, its utilization droped to ~80%. It agreed well with the batch system and evidenced the detrimental effect of excess H_2O_2. A low flow rate could enhance the contact time between the catalyst, H_2O_2, and the contaminants inside the filter [9]. As a result, MB degradation and H_2O_2 utilization tended to be similar to the initial stage and maintained at high values above 90%. However, MB degradation declined within the first 30 h when double MB was used, whereas it can be recovered and kept at high values in the following filtration. This self-adaptability may allow the filter to be used in actual wastewater treatment under broad conditions.

The MB solution was spiked with the effluent wastewater and subsequently passed through the filter. High MB degradation and H_2O_2 utilization efficiencies were all achieved (Fig. 3e). The outstanding performance of the filter could be ascribed to its three advantages. The first is the micropore structure of the catalyst- decorated filter, where the pollutant can be removed layer by layer within a comparable reaction time (calculated as ~17 min). This model facilitates rapid flow of

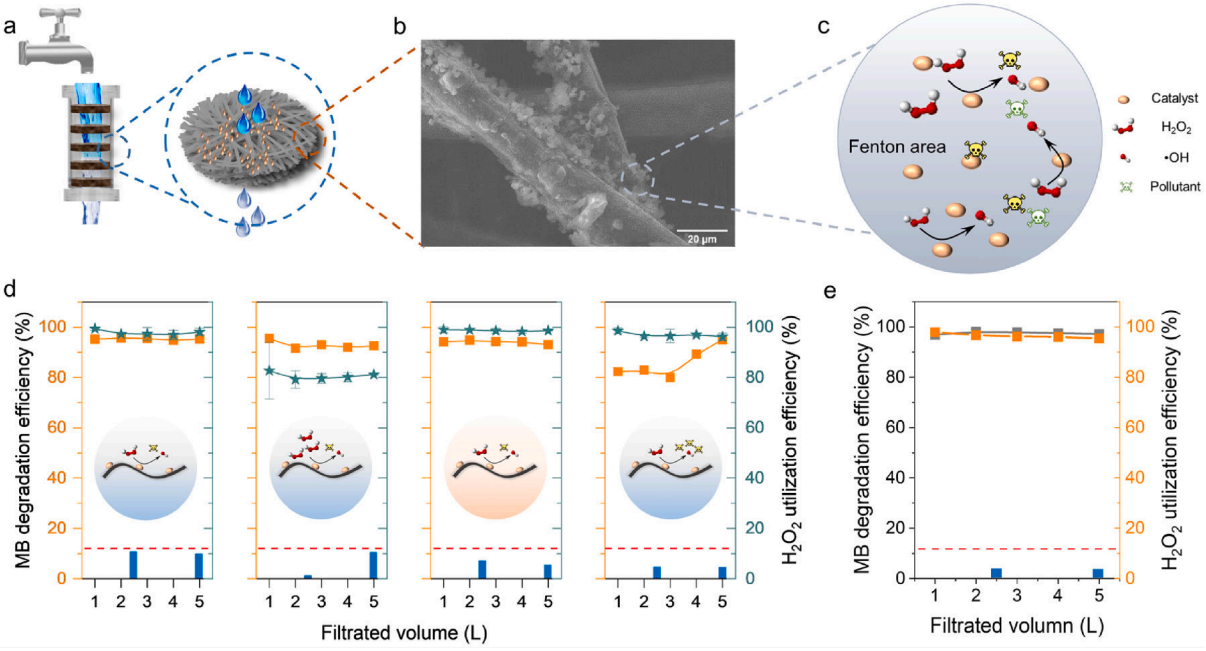

Fig. 3. (a) Schematic, (b) SEM image, and (c) catalytic mechamism of the flow-through filter. (d) MB degradation (10 mg/L) and H_2O_2 (2.625 mM) utilization efficiencies at a flow rate of 0.1 L/h during the first, the second (3.5 mM H_2O_2), the third (flow rate of 0.05 L/h), and the last filtration process (20 mg/L MB). The inset pictures illustrate different reaction that occurr in the corresponding process. (e) MB degradation and H_2O_2 utilization efficiencies during the filtration of the mixed wastewater. The blue bars indicate the Fe leaching during these filtration processes, and the red line represents 1 mg/L of Fe ions. (For interpretation of the references to color in this figure legend, the reader is referred to the web version of this article.)

wastewater and reduces the long-term exposure of the catalyst in harsh environments. However, in the batch system, the catalyst was fully immersed in the solution. As a result, the active sites on the catalyst surface could be covered by the catalyst aggregates and poisoned by complex compounds [26]. The second is enhanced mass transport and surface/interface contact. Low chemical diffusion in the batch system limited efficient contact between chemicals (H_2O_2 and pollutants) and the catalyst (Fig. S11) [8]. The instantaneous efficacy of $^{\bullet}OH$ (<10 μs) also cannot oxidize distant pollutants (>25 nm) [8]. The mass transport in the flow-through system can be restricted to a critical scale, maximizing the contact between chemicals and active sites and shortening radical migration distances (Fig. 3c). The third advantage is the leaching resistance of the filter. The Fe leaching in the filtrated water was all below 0.1 mg/L during the filtration process. Notably, when its concentration was gradually reduced to 0.031 mg/L, the filter still maintained high efficacy in actual wastewater treatment (Fig. 3e). Therefore, we demonstrated the applicability of the flow-through filter to real wastewater with low-dose H_2O_2 input.

3.3. Electrochemical integration system for wastewater treatment

3.3.1. Controllable in-situ generation of H_2O_2

One of the major challenges for in-situ electrochemical synthesis of H_2O_2 is to achieve its long-term stability [16]. Benefiting from the low H_2O_2 requirement (0.875–2.265 mM) in the above system, we, therefore, focused on the long-term continuous generation of H_2O_2 in this section. As shown in Fig. 4a, a full-body functional cathode was simply constructed by hydrophobic engineering of the cathode catalyst, addressing the low oxygen transfer and utilization issues of classical cathodes with a single catalytic layer. SEM images show that smooth PFTE slices form an interconnected porous layer on CF, and the porosity decreases from 25.41% to 2.24% with increasing PTFE concentration (0–8%, Fig. S12). However, the hydrophobicity of the electrode increased, suggested by the increased contact angle (107.21–132.44°, Fig. 4b). The LSVs of the cathodes were investigated to evaluate their electrochemical activity. We found that the highest current was achieved by 5% PTFE modification, which could be beneficial for the formation of sufficient reaction sites and rapid oxygen diffusion (Fig. S13a). The yield of H_2O_2 showed a similar tendency to the LSV results, with the accumulated H_2O_2 reached 1.48 mM within 1 h on the 5% PTFE modified cathode, which was 194% higher than the blank cathode (Fig. 4c). However, the synthesis of H_2O_2 was inhibited by the 8% PTFE modified cathode, confirming the unfavorable of excessive PTFE for H_2O_2 generation. In addition to the cathode design, an active and stable anode is also important for long-term operation. We compared three types of anodes and found that commercial IrO_2/Ti had the best electrochemical activity and the highest accumulated H_2O_2 (Fig. S13b–c). Moreover, the impact of operating conditions on system performance was evaluated. Clearly, the external voltage available to synthesize H_2O_2 started from 1.5 V and reached the highest yield at 2.0 V (Fig. S13d). A further increase in voltage resulted in low H_2O_2 accumulation, probably due to the decomposition of H_2O_2 under this condition [16]. We also noticed that acidic conditions favored H_2O_2 generation, but even in the neutral solution we still obtained a comparable yield (0.86 mM) close to our target range (0.875–2.265 mM, Fig. S13e).

The stability of the electro-synthesis system was tested in continuous flow mode. We ran the H_2O_2 generation cell by changing the external voltage, catholyte concentration, and flow rate (Fig. 4d). The H_2O_2 concentration was gradually increased, and even at a high flow rate (0.24 L/h), we still obtained a similar accumulated value after 24 h (1.60 mM). This concentration was in the proper range and not negatively affected by system parameters. Based on the optimal conditions,

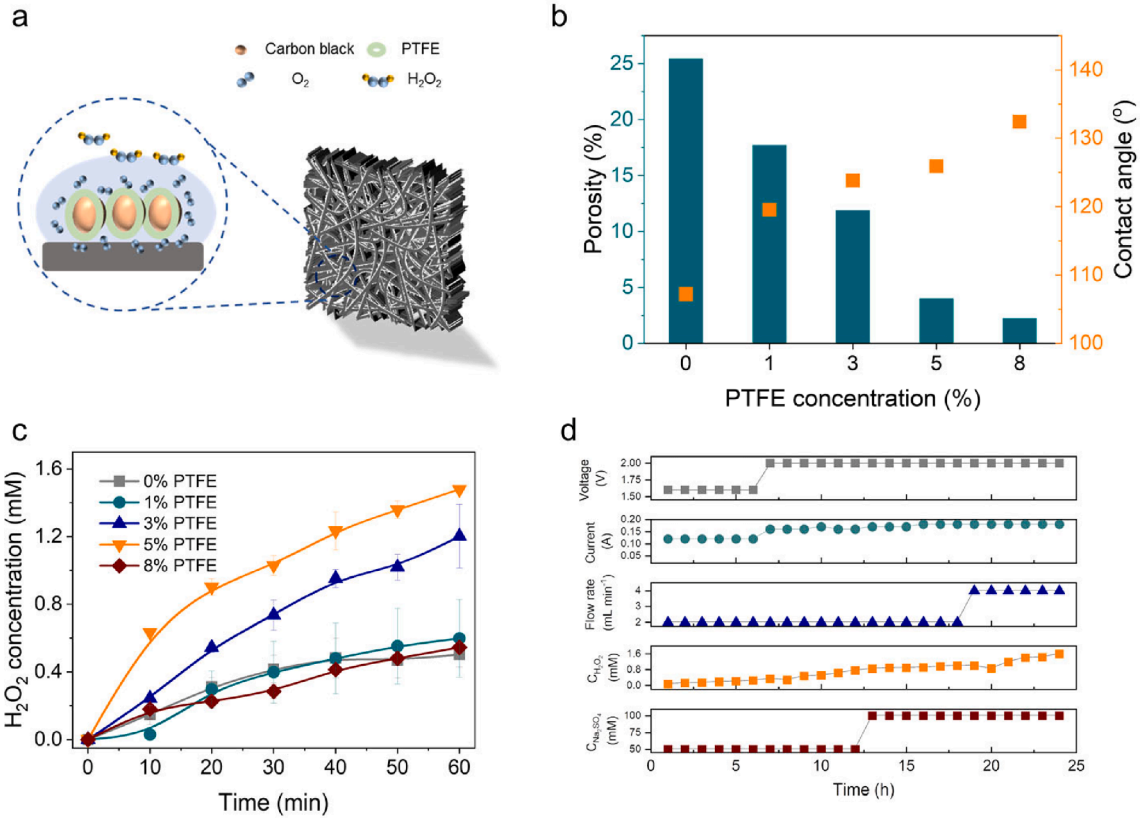

Fig. 4. (a) Illustration of the full-body engineered cathode for $2e^-$ ORR reaction. (b) Porosity and contact angle of the cathodes modified with different rates of PTFE. (c) H_2O_2 generation in the electrochemical system with different cathodes. (d) Continuous-flow generation of H_2O_2 in the electrochemical system by changing voltage, flow rate, and Na_2SO_4 concentration.

we further conducted a long-term flow experiment over 320 h (the highest reported operation time to our knowledge), which confirmed the high efficiency and long-term stability of the system (Fig. S13f).

3.3.2. Performance of the integrated system

We constructed an integrated system by combing the Fenton filter and the H_2O_2 generation cell. As illustrated in Fig. 5a, this system was operated in three steps: (1) H_2O_2 was controllably produced in an electrochemical generator; (2) the produced H_2O_2 was mixed with wastewater thoroughly; and (3) the mixed solution flowed through the FeN_x filter for final organic oxidation. All processes were driven by a pump and run simultaneously. Similarly, we operated the integrated system under different conditions and detected H_2O_2 and MB concentrations before and after the Fenton-like reaction. Firstly, the electrochemical H_2O_2 generatoration cell was set to an external voltage of 2.0 V and used 0.05 M Na_2SO_4 catholyte at a flow rate of 0.1 L/h. The effluent concentration of H_2O_2 was gradually increased to 1.45 mM after 50 h. Then it was mixed with synthetic MB wastewater (10 mg/L, pH 7) and flowed through the filter in single-pass mode. After the Fenton reaction inside the filter, H_2O_2 was consumed by 93.20–99.06% (Fig. 5b). Meanwhile, MB was also rapidly removed, and the efficiency maintained in the range of 80.10–98.40% (Fig. 5c). Then we restarted the system at a low flow rate (0.05 L/h) and noticed that it had no significant effect on H_2O_2 generation before (1.60 mM max) and after (0.27 mM max) the filtration (Fig. S14a). Consequently, we obtained a similar trend of degradation efficiency, with a slightly decrease from 98.36% to 87.53% (Fig. S14b). To further improve the system efficacy, we flowed double catholyte (0.1 M) into the cell. Unsurprisingly, H_2O_2 production was enhanced by 2.44–5.09 folds, yet we did not detect high H_2O_2 residue after the flow through (Fig. S14c). The degradation of MB was above 90% during the whole process (Fig. S12d). Moreover, we also observed nearly 100% H_2O_2 utilization and MB degradation if we decreased the concentration of MB (5 mg/L, Fig. S15a-b). Similar to the single flow-through system, Fe leaching in these processes was all below 0.1 mg/L (Fig. S15c), confirming the leaching resistance of the filter.

To investigate the stability of the novel system, we operated it under the optimal condition (voltage of 2 V, flow rate of 0.1 L/h, and 0.1 M Na_2SO_4). As shown in Fig. 5d, MB degradation and H_2O_2 utilization efficiencies all reached ~ 100% and kept stable after 500 h. Moreover, the system also showed a great application potential in actual wastewater treatment (Fig. 5e). Since we used the same filter as the above flow-through reactor, the integrated system exhibited similar performance in wastewater treatment (94.27–97.01%) and H_2O_2 utilization (84.45–97.19%). Overall, this novel system has three innovations. One is the high activity and wide adaptability of the catalyst-modified filter, which could be used to treat various types of organic wastewater. The second is the long-term stability of the H_2O_2 generatoration cell, which can be easily operated to achieve the target H_2O_2 concentration by changing the external conditions. Finally, the entire process is highly controllable, allowing us to adjust each process individually for complete pollutant removal and H_2O_2 utilization.

3.4. Comprehensive comparison of the three systems

3.4.1. Comparison of efficiency and sustainability

We compared the batch, flow-through, and integrated systems in terms of efficacy, sustainability, application potential, and total cost. To better understand their differences in efficacy, the degradation rates of MB were normalized in the same unit (mg_{MB}^{-1} min^{-1} $g_{catalyst}^{-1}$). Generally, the batch system showed different ranges of rates under different conditions (Fig. 6a). Especially the pH (0.99–1.93 mg_{MB}^{-1} min^{-1} $g_{catalyst}^{-1}$) and the catalyst content (1.93–4.56 mg_{MB}^{-1} min^{-1} $g_{catalyst}^{-1}$) had significant impacts on system performance. In contrast, the flow-through and integrated systems showed relatively stable efficacies under each condition (e.g., flow rate). We also observed the minimum difference in the last system, where all degradation rates were distributed in the same range (0.78–1.54 mg_{MB}^{-1} min^{-1} $g_{catalyst}^{-1}$). We used fresh catalyst in the batch system under different conditions, whereas the same catalyst-modified filter was assembled in the latter two systems and used throughout the treatment process. This is the main reason why the batch system showed better degradation rates. In fact, its activity dropped sharply after repeated use twice. As seen in Fig. 6b, the degradation rate was reduced by 7.72-fold (from 1.93 to 0.25 mg_{MB}^{-1} min^{-1} $g_{catalyst}^{-1}$). However, we did not observe any activity decency in the flow-though and integration systems. Note that the degradation rates of these two systems were ~ 558.33% higher than that of the batch system after three

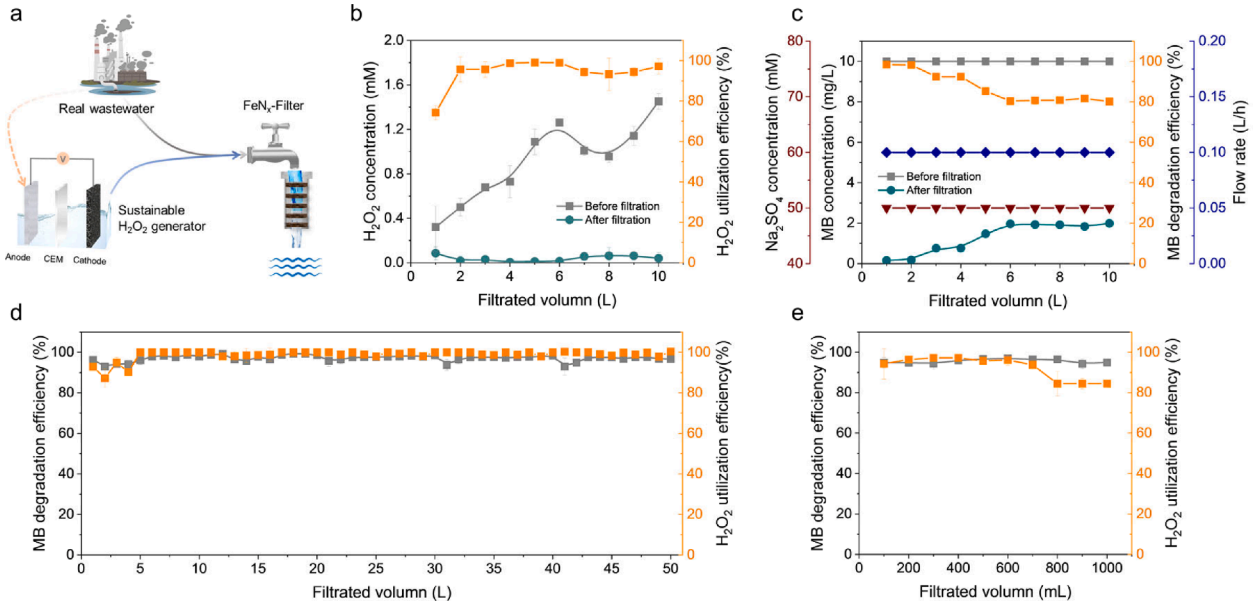

Fig. 5. (a) Schematic of the integrated electrochemical system for wastewater treatment. (b) Changes in H_2O_2 and (c) MB concentration before and after filtration, and MB degradation and H_2O_2 utilization efficiencies during the whole filtration process. (d) MB degradation and H_2O_2 utilization efficiencies in the long-term continuous-flow system and (e) in the filtration of the mixed effluent wastewater. Conditions: external voltage (2.0 V), flow rate (0.1 L/h), MB concentration (10 mg/L), and Na_2SO_4 concentration (0.05 M) if not otherwise specialized.

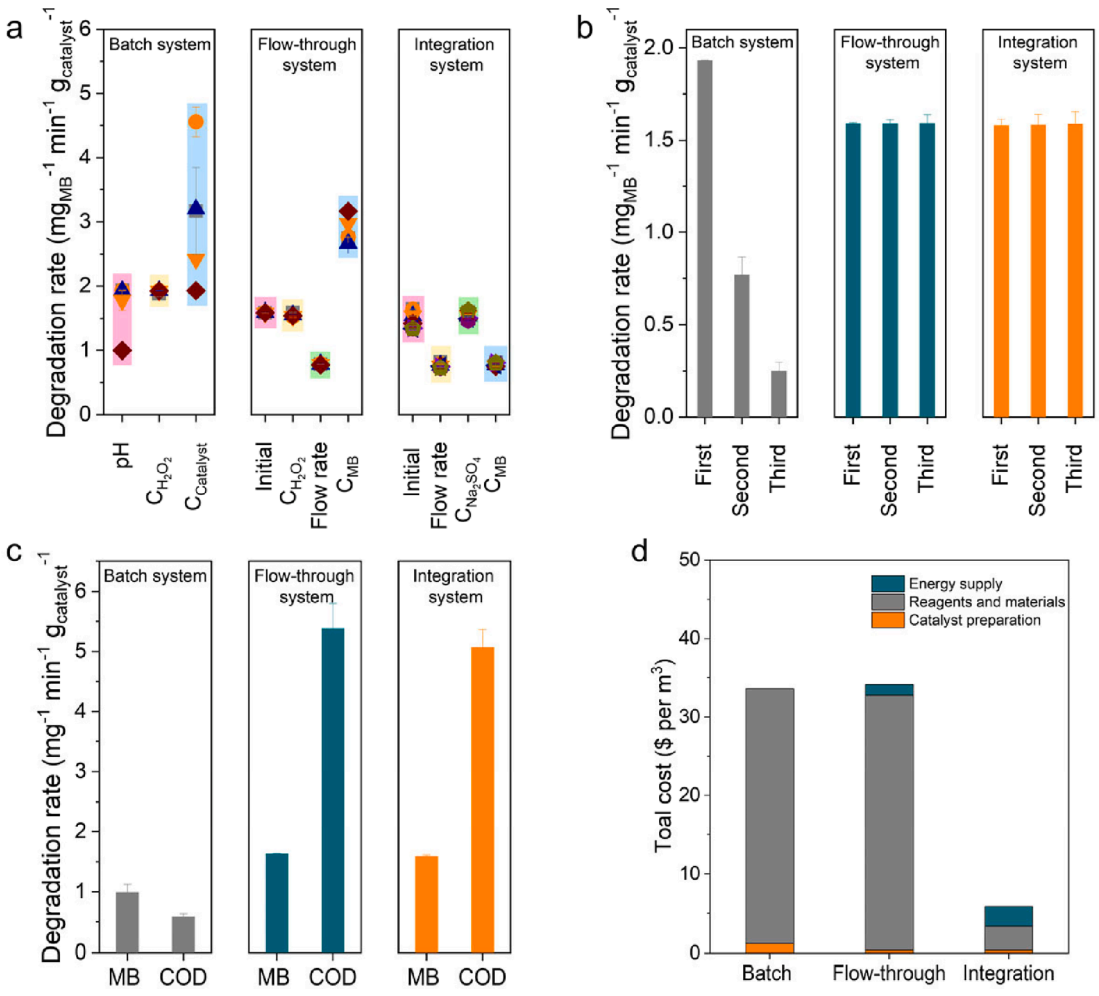

Fig. 6. (a) Comparison of the batch, flow-through, and integration systems in terms of (a) efficacy, (b) sustainability, (c) application potential, and (d) total cost.

cycles, affirming their ultrahigh sustainability. As mentioned above, this excellent ability can be attributed to the low loss of the catalyst-modified filter and the long-term stability of the H_2O_2 generation cell especially when they were operated in continuous-flow mode. Note that low flow rates and three-cycle experiments are insufficient for practical large-scale applications, but this integrated system was developed for a proof-of-concept study showing its high durability at the current stage. Future work will focus on scaling-up applications for long-term tests over months or even years.

3.4.2. *Evaluation of application potential and cost*

The major limitation of Fenton/Fenton-like catalysts in wastewater treatment is their low potential for real-world application. We observed similar results in the batch system, as the MB degradation rate reduced by 2.03 folds with the existence of actual wastewater (Fig. S8b). Meanwhile, the total COD removal rate was as low as 0.59 mg_{COD}^{-1} min^{-1} $g_{catalyst}^{-1}$ (Fig. 6c). However, this can be alleviated by the filter device as MB degradation and COD removal rates were enhanced to 1.62 and 5.37 mg^{-1} min^{-1} $g_{catalyst}^{-1}$, respectively. Using the same filter as the Fenton generator, the integrated system also showed high degradation rates for MB (1.59 mg_{MB}^{-1} min^{-1} $g_{catalyst}^{-1}$) and effluent wastewater (5.07 mg_{COD}^{-1} min^{-1} $g_{catalyst}^{-1}$). More importantly, the Fenton process performed in this continuous unit can treat large volumes of wastewater without the need to separate and recover catalyst. The controllable H_2O_2 generatoration cell could also be operated for a long time, which solved the problem of continuous dosing and waste of reagents. It is worth mentioning that various complex organic and inorganic compounds in actual wastewater may cover the active sites on the electrode or the filter during long-term operation, thereby inhibiting the performance of the integrated system. It should be overcome in the future. We also assessed the total cost of these lab-scale wastewater treatment systems. In general, the cost mainly comes from catalyst preparation, energy supply, and reagents and materials (Fig. 6d). Due to the need for more fresh catalyst, the cost of catalyst preparation for the batch system was higher than the other two systems. In contrast, the flow-through and integrated systems spent more on energy supply, including external voltage and pump. Most of the cost was spent on reagents and materials. Among them, expensive H_2O_2 was added to the batch and flow-through systems, accounting for >90% of the total cost. When we introduced the H_2O_2 generatorion cell, only low catholyte concentration and moderate external voltage were required for H_2O_2 synthesis. Therefore, the low-cost catholyte is one of the main advantages of the integrated system for wastewater treatment. Moreover, we should note that the filter reactor and the H_2O_2 generation cell need to be upgraded to adapt to large-scale applications. Firstly, the synthesis of inexpensive and easily prepared catalysts will remain a future goal since we used high temperature to synthesize the catalyst. Secondly, various commercial materials (e.g., corundum ball) should also be explored to efficiently immobilize catalysts as filters or electrodes to improve their long-term stability.

4. Conclusions

This work accurately controlled the ratio of precursors to obtain subnano FeN_x clusters. $FeN_{1.0}$ showed excellent activity and stability to

remove multiple contaminants under different conditions, but it was inhibited in actual wastewater due to excessive exposure to active sites. A simple Fenton filter was developed to solve this issue and achieved high pollutant degradation and H_2O_2 utilization. Moreover, an electrosynthesis system was constructed with a full-body engineered cathode and used for long-term in-situ H_2O_2 generation. We finally integrated a novel system by combing the filter and electrochemical H_2O_2 generation cell. This integration system can realize wastewater treatment with high efficiency, stability, broad application potential, and low cost. The findings present a promising path for achieving practical application of metal clusters in sustainable systems.

CRediT authorship contribution statement

Biao Li: Investigation, Methodology, Validation, Formal analysis, Writing – original draft. **Rusen Zou:** Writing – review & editing. **Yanyan Su:** Supervision, Writing – review & editing. **Yifeng Zhang:** Conceptualization, Supervision, Resources, Funding acquisition, Writing – review & editing.

Declaration of Competing Interest

The authors declare that they have no known competing financial interests or personal relationships that could have appeared to influence the work reported in this paper.

Data availability

Data will be made available on request.

Acknowledgements

The authors gratefully acknowledge the financial support from China Scholarship Council. The authors would like to thank Pengxuan Zheng from Shiyanjia Lab (www.shiyanjia.com) for the EPR analysis. This work was financially supported by the Carlsberg Foundation Distinguished Fellowships (CF18-0084, Denmark).

Appendix A. Supplementary material

Supplementary material to this article can be found online at https://doi.org/10.1016/j.seppur.2022.122372.

References

[1] H. Song, R. Du, Y. Wang, D. Zu, R. Zhou, Y. Cai, F. Wang, Z. Li, Y. Shen, C. Li, Anchoring single atom cobalt on two-dimensional MXene for activation of peroxymonosulfate, Appl. Catal. B 286 (2021).
[2] Y. Long, J. Dai, S. Zhao, Y. Su, Z. Wang, Z. Zhang, Atomically dispersed cobalt sites on graphene as efficient periodate activators for selective organic pollutant degradation, Environ. Sci. Technol. 55 (2021) 5357–5370.
[3] Y. Gao, T. Wu, C. Yang, C. Ma, Z. Zhao, Z. Wu, S. Cao, W. Geng, Y. Wang, Y. Yao, Y. Zhang, C. Cheng, Activity trends and mechanisms in peroxymonosulfate-assisted catalytic production of singlet oxygen over atomic metal-n-c catalysts, Angew. Chem. Int. Ed. 60 (2021) 22513–22521.
[4] J. Xu, X. Zheng, Z. Feng, Z. Lu, Z. Zhang, W. Huang, Y. Li, D. Vuckovic, Y. Li, S. Dai, G. Chen, K. Wang, H. Wang, J.K. Chen, W. Mitch, Y. Cui, Organic wastewater treatment by a single-atom catalyst and electrolytically produced H_2O_2, Nat. Sustain. 4 (2020) 233–241.
[5] C. Shan, H. Liu, M. Hua, B. Pan, Enhanced Fenton-like oxidation of As (III) over Ce–Ti binary oxide: A new strategy to tune catalytic activity via balancing bimolecular adsorption energies, Environ. Sci. Technol. 54 (2020) 5893–5901.
[6] J. Zhu, X. Zhu, F. Cheng, P. Li, F. Wang, Y. Xiao, W. Xiong, Preparing copper doped carbon nitride from melamine templated crystalline copper chloride for Fenton-like catalysis, Appl. Catal. B 256 (2019).
[7] M. Liu, Z. Feng, X. Luan, W. Chu, H. Zhao, G. Zhao, Accelerated Fe^{2+} regeneration in an effective electro-fenton process by boosting internal electron transfer to a nitrogen-conjugated Fe (III) complex, Environ. Sci. Technol. 55 (2021) 6042–6051.
[8] D. Guo, Y. Liu, H. Ji, C.C. Wang, B. Chen, C. Shen, F. Li, Y. Wang, P. Lu, W. Liu, Silicate-enhanced heterogeneous flow-through electro-fenton system using iron oxides under nanoconfinement, Environ. Sci. Technol. 55 (2021) 4045–4053.
[9] F. Liu, Y. Liu, Q. Yao, Y. Wang, X. Fang, C. Shen, F. Li, M. Huang, Z. Wang, W. Sand, Supported atomically-precise gold nanoclusters for enhanced flow-through electro-Fenton, Environ. Sci. Technol. 54 (2020) 5913–5921.
[10] M. Cheng, G. Zeng, D. Huang, C. Lai, Y. Liu, C. Zhang, J. Wan, L. Hu, C. Zhou, W. Xiong, Efficient degradation of sulfamethazine in simulated and real wastewater at slightly basic pH values using Co-SAM-SCS/H_2O_2 Fenton-like system, Water Res. 138 (2018) 7–18.
[11] Q. Yan, C. Lian, K. Huang, L. Liang, H. Yu, P. Yin, J. Zhang, M. Xing, Constructing an acidic microenvironment by MoS_2 in heterogeneous fenton reaction for pollutant control, Angew. Chem. Int. Ed. Engl. 60 (2021) 17155–17163.
[12] Y. Bao, C. Lian, K. Huang, H. Yu, W. Liu, J. Zhang, M. Xing, Generating High-valent Iron-oxo≡FeIV=O complexes in neutral microenvironments through peroxymonosulfate activation by Zn−Fe layered double hydroxides, Angew. Chem. Int. Ed. (2022).
[13] Y. Mao, P. Wang, D. Zhang, Y. Xia, Y. Li, W. Zeng, S. Zhan, J.C. Crittenden, Accelerating Fe(III)-aqua complex reduction in an efficient solid-liquid-interfacial Fenton reaction over the Mn-CNH co-catalyst at near-neutral pH, Environ. Sci. Technol. 55 (2021) 13326–13334.
[14] Y. Liu, Y. Chen, J. Deng, J. Wang, N-doped aluminum-graphite (Al-Gr-N) composite for enhancing in-situ production and activation of hydrogen peroxide to treat landfill leachate, Appl. Catal. B 297 (2021).
[15] L. Hu, G. Zhang, M. Liu, Q. Wang, P. Wang, Enhanced degradation of Bisphenol A (BPA) by peroxymonosulfate with Co_3O_4-Bi_2O_3 catalyst activation: effects of pH, inorganic anions, and water matrix, Chem. Eng. J. 338 (2018) 300–310.
[16] Y. Xia, X. Zhao, C. Xia, Z.Y. Wu, P. Zhu, J.Y.T. Kim, X. Bai, G. Gao, Y. Hu, J. Zhong, Y. Liu, H. Wang, Highly active and selective oxygen reduction to H_2O_2 on boron-doped carbon for high production rates, Nat. Commun. 12 (2021) 4225.
[17] X. Zhang, Y. Xia, C. Xia, H. Wang, Insights into practical-scale electrochemical H_2O_2 synthesis, Trends in Chemistry 2 (2020) 942–953.
[18] C. Xia, Y. Xia, P. Zhu, L. Fan, H. Wang, Direct electrosynthesis of pure aqueous H_2O_2 solutions up to 20% by weight using a solid electrolyte, Science 366 (2019) 226–231.
[19] W. Zhou, L. Xie, J. Gao, R. Nazari, H. Zhao, X. Meng, F. Sun, G. Zhao, J. Ma, Selective H_2O_2 electrosynthesis by O-doped and transition-metal-O-doped carbon cathodes via O_2 electroreduction: a critical review, Chem. Eng. J. (2021) 128368.
[20] R. Zou, A. Hasanzadeh, A. Khataee, X. Yang, M. Xu, I. Angelidaki, Y. Zhang, Scaling-up of microbial electrosynthesis with multiple electrodes for in situ production of hydrogen peroxide, Iscience 24 (2021), 102094.
[21] Y. Gao, C. Yang, M. Zhou, C. He, S. Cao, Y. Long, S. Li, Y. Lin, P. Zhu, C. Cheng, Transition metal and Metal–Nx codoped MOF-derived Fenton-like catalysts: A comparative study on single atoms and nanoparticles, Small 16 (2020) 2005060.
[22] W. Miao, Y. Liu, D. Wang, N. Du, Z. Ye, Y. Hou, S. Mao, K.K. Ostrikov, The role of Fe-Nx single-atom catalytic sites in peroxymonosulfate activation: Formation of surface-activated complex and non-radical pathways, Chem. Eng. J. 423 (2021), 130250.
[23] Y. Yin, W. Li, C. Xu, L. Shi, L.-C. Zhang, Z. Ao, M. Liu, M. Lu, X. Duan, S. Wang, Ultrafine copper nanoclusters and single sites for Fenton-like reactions with high atom utilities, Environmental Science, Nano 7 (2020) 2595–2606.
[24] J. Zhang, Y. Nosaka, Quantitative detection of OH radicals for investigating the reaction mechanism of various visible-light TiO_2 photocatalysts in aqueous suspension, J. Phys. Chem. C 117 (2013) 1383–1391.
[25] D. Trpkov, M. Panjan, L. Kopanja, M. Tadić, Hydrothermal synthesis, morphology, magnetic properties and self-assembly of hierarchical α-Fe_2O_3 (hematite) mushroom-, cube-and sphere-like superstructures, Appl. Surf. Sci. 457 (2018) 427–438.
[26] B. Li, X. Cheng, R. Zou, X. Yong, C. Pang, Y. Su, Y. Zhang, Simple modulation of Fe-based single atoms/clusters catalyst with acidic microenvironment for ultrafast Fenton-like reaction, Appl. Catal. B 304 (2022), 121009.
[27] H. Cao, J. Wang, J.-H. Kim, Z. Guo, J. Xiao, J. Yang, J. Chang, Y. Shi, Y. Xie, Different roles of Fe atoms and nanoparticles on g-C3N4 in regulating the reductive activation of ozone under visible light, Appl. Catal. B 296 (2021).
[28] S. An, G. Zhang, T. Wang, W. Zhang, K. Li, C. Song, J.T. Miller, S. Miao, J. Wang, X. Guo, High-density ultra-small clusters and single-atom Fe sites embedded in graphitic carbon nitride (g-C_3N_4) for highly efficient catalytic advanced oxidation processes, ACS Nano 12 (2018) 9441–9450.
[29] G. Lei, W. Zhao, L. Shen, S. Liang, C. Au, L. Jiang, Isolated iron sites embedded in graphitic carbon nitride (g-C_3N_4) for efficient oxidative desulfurization, Appl. Catal. B 267 (2020).
[30] W. Miao, Y. Liu, D. Wang, N. Du, Z. Ye, Y. Hou, S. Mao, K. Ostrikov, The role of Fe-Nx single-atom catalytic sites in peroxymonosulfate activation: Formation of surface-activated complex and non-radical pathways, Chem. Eng. Sci. 423 (2021).
[31] L. Peng, X. Duan, Y. Shang, B. Gao, X. Xu, Engineered carbon supported single iron atom sites and iron clusters from Fe-rich Enteromorpha for Fenton-like reactions via nonradical pathways, Appl. Catal. B 287 (2021).
[32] G. Nie, K. Hu, W. Ren, P. Zhou, X. Duan, L. Xiao, S. Wang, Mechanical agitation accelerated ultrasonication for wastewater treatment: Sustainable production of hydroxyl radicals, Water Res. 198 (2021), 117124.
[33] H. Wang, T. Chen, D. Chen, X. Zou, M. Li, F. Huang, F. Sun, C. Wang, D. Shu, H. Liu, Sulfurized oolitic hematite as a heterogeneous Fenton-like catalyst for tetracycline antibiotic degradation, Appl. Catal. B 260 (2020).
[34] L. Chen, S. Wang, Z. Yang, J. Qian, B. Pan, Selective interfacial oxidation of organic pollutants in Fenton-like system mediated by Fe(III)-adsorbed carbon nanotubes, Appl. Catal. B 292 (2021).